Quantum Information Processing (2025) 24:400
https://doi.org/10.1007/s11128-025-05017-9

A framework for quantum controlled teleportation in multi-hop networks: noise analysis and IBMQ evaluation

Mahla Moridi Farimani[1] · **Yousef Mafi**[1]

Received: 14 July 2025 / Accepted: 29 November 2025

Abstract
Multi-hop quantum teleportation is a fundamental technique for enabling scalable, long-distance quantum communication, making it a key building block for future quantum networks. In this paper, we present a generalized multi-hop quantum controlled teleportation (MQCT) protocol that enables more flexible transfer across complex network architectures. We perform a detailed analysis of the protocol's performance under realistic noise conditions, focusing on the impact of various noise sources on both the teleportation process and the underlying quantum channels. To assess its practical performance, we implemented the protocol on an IBM quantum (IBMQ) computer. The experimental results demonstrate the feasibility of the protocol in near-term quantum devices and provide valuable insights into its behavior under real-world quantum noise, paving the way for more reliable quantum communication systems.

Keywords Quantum communication · Quantum teleportation · Multi-hop quantum controlled teleportation · IBMQ computer · Quantum noise analysis

1 Introduction

Quantum physics introduces novel approaches to creating, transmitting, manipulating, and storing information by leveraging quantum phenomena. Quantum communication [1], a burgeoning area within quantum information, is essential for the development of future quantum networks, including the quantum Internet and quantum wireless networks [2], regardless of whether the communication occurs over short distances, such as centimeters, or spans thousands of kilometers.

Extending this perspective, the concept of distributed gate-model quantum computing [3–5] together with quantum networking is regarded as a pathway to surpass the inherent limits of isolated devices. By linking multiple processors, such systems could achieve scalable computation while simultaneously enabling secure communication channels. The eventual emergence of a quantum internet [6–8] would not only connect

✉ Yousef Mafi
yousef.mafi@tuni.fi

[1] Faculty of Engineering and Natural Sciences, Tampere University, Tampere, Finland

distant quantum nodes but also facilitate the execution of distributed algorithms and support cryptographic schemes resistant to classical attacks. In the longer term, these capabilities are expected to form the basis of a global quantum infrastructure with a significant impact on areas such as large-scale simulation, complex optimization, and secure information exchange.

Quantum teleportation (QT) [9] is a key technique that enables such communication. It relies on a special type of bipartite maximally entangled state known as a Bell pair, in which two spatially separated quantum systems are linked by a nonlocal correlation, often referred to by Einstein as "spooky action at a distance." While long-distance quantum teleportation has been demonstrated experimentally since its first realization in 1997, the communication distance remains constrained due to losses in quantum channels [10]. This limitation can be mitigated through entanglement swapping [11], a process that establishes entanglement between distant nodes via intermediate nodes.

Quantum teleportation covers a variety of research topics, each addressing different facets and uses of this key quantum phenomenon [12–16]. Notable areas of study include multi-party teleportation [17–24], where the transfer of quantum states involves more than two participants, and controlled teleportation, which introduces the ability for one party to manage the teleportation process. Furthermore, multi-hop teleportation enables quantum communication over longer distances by using intermediate nodes, whereas continuous-variable teleportation focuses on quantum systems that use continuous variables rather than discrete qubits. These approaches deepen our understanding of teleportation and open new possibilities for real-world applications in quantum networks, cryptography, and computing [25].

Recent advances in quantum communication have predominantly focused on two-party quantum teleportation protocols, leaving network-oriented schemes relatively underexplored. To bridge this gap, several studies have proposed routing mechanisms that support wireless quantum state transmission across interconnected quantum devices. Such frameworks have been experimentally and theoretically examined in distributed wireless quantum networks, particularly through multi-hop communication schemes involving entangled Bell pairs.

Efforts to enhance state transfer fidelity in these settings have led to the investigation of partially entangled channels and Werner states as mediators for hop-by-hop teleportation [25, 26]. These protocols have been implemented in various topological configurations, including mesh networks and measurement-device-independent (MDI) architectures [18, 27, 28]. Diverse classes of entangled resources have been utilized in these contexts, such as GHZ–Bell hybrid states [19, 20], asymmetric W states [21], and cluster-type entangled states [22], each offering unique trade-offs in terms of entanglement distribution, robustness, and network scalability.

Expanding on this foundation, Wu et al. [23] proposed a hierarchical multi-hop teleportation protocol that employs entanglement swapping with multiple Bell pairs to extend communication over greater distances. In a related development, Zhang et al. [24] introduced a deterministic bidirectional teleportation scheme within a multi-hop network, leveraging GHZ and Bell states as the fundamental shared resources. Their approach incorporated adaptive channel selection strategies based on the number of hops along the communication path, highlighting the influence of network topology on teleportation performance.

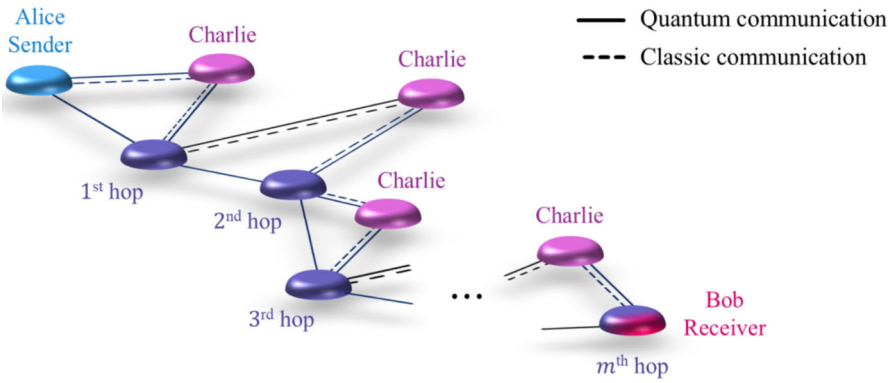

Fig. 1 Schematic representation of the proposed multi-hop quantum controlled teleportation (MQCT) protocol

In this study, we introduce a generalized protocol for multi-hop quantum controlled teleportation [17], aimed at developing a comprehensive, validated framework for multi-hop quantum networks. As depicted in Fig. 1, each hop in the network involves a controller, Charlie, who manages the flow of information during each teleportation event between adjacent nodes. A key consideration in this context is the trade-off between the number of hops m and the impact of quantum noise, such as noisy channels and operations. To address this, we conduct a thorough noise analysis across various network architectures, evaluating the reliability of the multi-hop teleportation concept. Additionally, leveraging the IBMQ platform enables validation of the proposed protocol on a real quantum system. Our findings demonstrate that multi-hop teleportation is not only feasible and reliable but can also be effectively controlled with high fidelity across multiple hops.

The paper is organized as follows: Sec. 2 presents the generalized protocol, supported by mathematical proofs. Section 3 introduces the quantum noise model and investigates its effects on the transferred state in noisy quantum channels and operations. In Sec. 4, the results of implementing the protocol on the IBM Quantum computer are presented for various architectures. Section 5 discusses the results, provides an outlook for future research, and concludes with a summary of key findings in Sec. 6.

2 Quantum controlled teleportation protocol framework

Quantum teleportation enables the faithful transfer of an unknown single-qubit state from a sender (Alice) to a distant receiver (Bob) without physically transmitting the qubit itself. In the standard protocol, Alice and Bob preshare a Bell pair, which is maximally entangled. Alice performs a joint Bell-state measurement on her half of the pair and the input qubit, and then forwards the two-bit outcome to Bob via a classical channel. Bob applies the corresponding Pauli correction to his qubit, recovering the original state at his location.

Quantum controlled teleportation (QCT) follows the same fundamental principles as standard QT, with the addition of a third party, called Charlie, who oversees and controls the teleportation process. In QCT, the quantum channel is composed of a Greenberger–Horne–Zeilinger (GHZ) state shared among Alice, Bob, and Charlie. After receiving Alice's measurement results, Charlie measures his own qubit and, based on the combined outcomes, informs Bob of the specific operations required to reconstruct the unknown input state.

In QCT, Alice intends to transmit an unknown quantum state, denoted $|\phi_A\rangle$, which is expressed as:

$$|\phi_A\rangle = \alpha_0|0\rangle + \alpha_1|1\rangle \tag{1}$$

where state coefficients are required to satisfy the normalization condition $\sum_i |\alpha_i|^2 = 1$.

The quantum channel is realized as a GHZ state, given by:

$$|\phi_{ch}\rangle = |\phi_{C^1 h^1 h'^1}\rangle = \frac{1}{\sqrt{2}}(|000\rangle + |111\rangle) \tag{2}$$

Accordingly, the initial state of the entire quantum system can be written as

$$|\psi_0\rangle = |\phi_A\rangle \otimes |\phi_{ch}\rangle \tag{3}$$

In the general QCT protocol, it is typically assumed that a single-hop structure exists, meaning only one teleportation step is required. The mathematical details and proof for the single-hop QCT case are provided in Appendix A.1.

Considering the overall QCT process as the application of a unitary operator U_{QCT}, the final state of the quantum system $|\psi_f\rangle$ after performing QCT on qubits $|\phi_A\rangle$, $|\phi_{C^1}\rangle$, $|\phi_{h^1}\rangle$, and $|\phi_{h'^1}\rangle$ can be written as:

$$|\psi_f\rangle = |\phi_{h'^1}\rangle = U_{QCT}|\psi_0\rangle = \alpha_0|0\rangle + \alpha_1|1\rangle \tag{4}$$

This result demonstrates that the unknown input state has been successfully transmitted to Bob within the single-hop QCT framework.

2.1 Multi-hop quantum controlled teleportation protocol

The proposed generalized protocol follows a procedure similar to the QCT protocol. As illustrated in Fig. 2, Alice can transmit an unknown input state to Bob through a quantum channel consisting of a m-hop network by sequentially applying multiple U_{QCT} operations. Specifically, at each stage, the quantum state is teleported from one hop to the next, and after an m number of U_{QCT} operations, the input state is successfully teleported to the final hop, corresponding to Bob.

The proposed MQCT protocol is formally described in Algorithm 2.1.

Considering Alice's input state given by Eq. 1, the generalized quantum channel is composed of m GHZ states, where each hop is associated with a distinct GHZ state

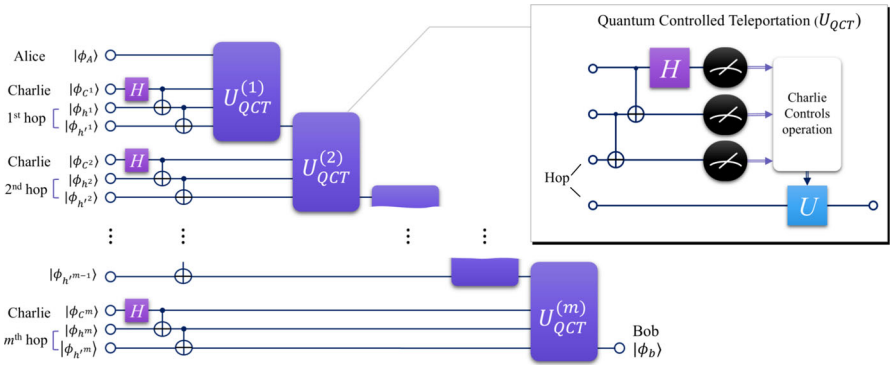

Fig. 2 Quantum circuit diagram of the proposed multi-hop quantum controlled teleportation protocol. The input quantum state is transmitted from Alice to Bob through an m-hop quantum channel, consisting of m sequential quantum controlled teleportation operations (U_{QCT})

Algorithm 1 Multi-hop Quantum Controlled Teleportation Protocol

Require: Alice holds a qubit on a unknown state $|\phi_A\rangle = \alpha_0|0\rangle + \alpha_1|1\rangle$. The quantum channel consists of m entangled GHZ states across nodes $C^1, h^1, h'^1, ..., C^m, h^m, h'^m$, expressed as $|\phi_{ch}\rangle = |\phi_{\text{GHZ}}\rangle^{\otimes m}$.
Ensure: The state $|\phi_A\rangle$ is transferred to Bob's qubit: $|\phi_A\rangle \rightarrow |\phi_{h'^m}\rangle$
% Initialization process
Alice possesses qubit A prepared in the state $|\phi_A\rangle$.
Charlie establishes the quantum channel: $|\phi_{C^1h^1h'^1}\rangle \otimes |\phi_{C^2h^2h'^2}\rangle \otimes ... \otimes |\phi_{C^mh^mh'^m}\rangle = |\phi_{\text{GHZ}}\rangle^{\otimes m}$
% Teleportation through the quantum channel consisted of m hops
repeat
    Apply **QCT**(Input qubit $|\phi_{in}\rangle$: $|\phi_{h'^{i-1}}\rangle$, Quantum channel $|\phi_{ch}\rangle$: $|\phi_{C^ih^ih'^i}\rangle$)
    $i \leftarrow i + 1$
until $i = m$
Result: Bob's qubit $|\phi_{h'^m}\rangle$ is now in state $|\phi_A\rangle \rightarrow |\phi_{h'^m}\rangle$.

% Single qubit quantum controlled teleportation function
function QCT(Input qubit $|\phi_{in}\rangle$, Quantum channel $|\phi_{ch}\rangle = |q_0q_1q_2\rangle$)
    Change measurement basis: $U^{\dagger}_{\text{GHZ}}|\phi_{in}\rangle|q_0q_1\rangle$
    Measuring qubits $|\phi_{in}\rangle$, $|\phi_{q_0}\rangle$, $|\phi_{q_1}\rangle$
    Send classical bits, $\mathcal{M}_{in}$ and $\mathcal{M}_{q_0}$, to Charlie
    if $\mathcal{M}_{in} == 1$ **then**
        Applying Z operator on $|\phi_{q_2}\rangle$
    else
        Applying I operator on $|\phi_{q_2}\rangle$
    end if
    if $\mathcal{M}_{q_0} == 1$ **then**
        Applying X operator on $|\phi_{q_2}\rangle$
    else
        Applying I operator on $|\phi_{q_2}\rangle$
    end if
end function

as follows:

$$|\phi_{ch}\rangle = |\phi_{C^1 h^1 h'^1}\rangle \otimes \cdots \otimes |\phi_{C^m h^m h'^m}\rangle = \left(\frac{1}{\sqrt{2}}(|000\rangle + |111\rangle)\right)^{\otimes m} \tag{5}$$

By applying m consecutive U_{QCT} operations, as depicted in Fig. 2, the final state of the system after teleportation can be expressed as:

$$|\psi_f\rangle = |\phi_{h'^m}\rangle = U^{(m)}_{QCT} \ldots U^{(1)}_{QCT} |\psi_{in}\rangle = \alpha_0|0\rangle + \alpha_1|1\rangle \tag{6}$$

This expression confirms that the unknown input state has been successfully transmitted to Bob through the m-hop quantum network. The mathematical proof and detailed analysis for the case of $m = 2$ are provided in Appendix A.2.

2.2 Generalization of the MQCT protocol

In the generalized version of the proposed MQCT protocol, Alice aims to transmit an unknown n-qubit state, denoted by $|\Phi_A\rangle$, to Bob through an m-hop quantum channel. The n-qubit input state is defined as:

$$|\Phi_A\rangle = |\phi_{A_1}\rangle \otimes \cdots \otimes |\phi_{A_n}\rangle = \sum_{i=0}^{2^n-1} \alpha_i |i\rangle \tag{7}$$

where the normalization condition $\sum_i |\alpha_i|^2 = 1$ is satisfied.

As depicted in Fig. 3, the quantum channel is structured such that each hop contains n GHZ states. Consequently, the complete quantum channel consists of a total of $n \times m$ GHZ states, which can be expressed as:

$$|\Phi_{ch}\rangle = |\phi_{ch}\rangle^{\otimes n} = \left(\left(\frac{1}{\sqrt{2}}(|000\rangle + |111\rangle)\right)^{\otimes m}\right)^{\otimes n} \tag{8}$$

The teleportation process follows the same principles as the MQCT protocol, with the distinction that it is generalized to n-qubit systems. To transmit the input state to Bob, the QCT protocol must be applied m times, once per hop. The generalized QCT operation $\mathbf{U}_{QCT}$, capable of teleporting n-qubit states. After completing this sequence of m $\mathbf{U}_{QCT}$ operations, the final state of the quantum system can be written as:

$$|\Psi_f\rangle = |\phi_{h_1'^m}\rangle \otimes \cdots \otimes |\phi_{h_n'^m}\rangle = \mathbf{U}^{(m)}_{QCT} \ldots \mathbf{U}^{(1)}_{QCT} |\psi_0\rangle = \sum_{i=0}^{2^n-1} \alpha_i |i\rangle \tag{9}$$

This result confirms that the unknown n-qubit input state is successfully transmitted to Bob over the m-hop quantum network.

In the subsequent sections, the proposed protocol is evaluated and validated for different values of m, representing the number of hops in the quantum network. To

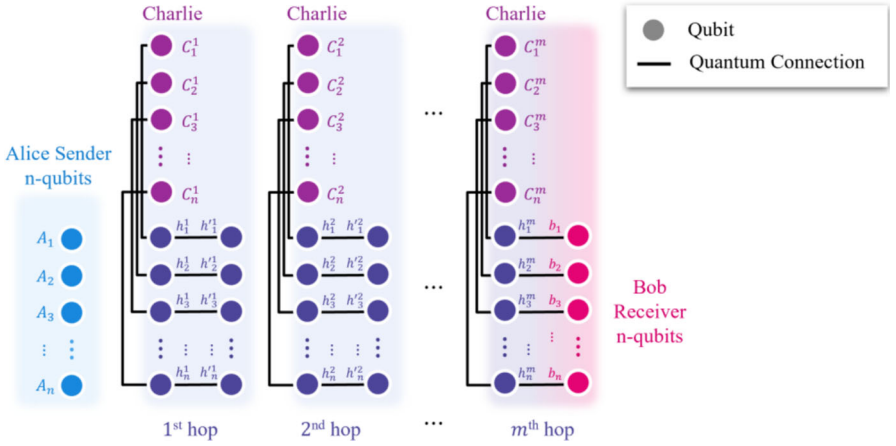

Fig. 3 Generalized schematic of the multi-hop quantum controlled teleportation protocol. An n-qubit input state $(A_1, ..., A_n)$ is transmitted from Alice to Bob over an m-hop quantum channel. Each hop utilizes an n-qubit GHZ state as the entangled quantum resource

gain insight into the behavior of higher-dimensional quantum systems ($n > 1$), we only analyze the protocol for the case where $n = 1$, corresponding to a single-qubit input state. This is justified by the fact that, in the generalized MQCT protocol, each input qubit is treated independently. Consequently, the teleportation of an n-qubit state can be viewed as n parallel single-qubit MQCT processes, collectively forming the generalized MQCT protocol.

3 Modeling and analysis of quantum noise effects

The formalism of quantum operations provides a versatile framework for describing the evolution of quantum systems under various conditions, including stochastic changes to quantum states, much as Markov processes describe stochastic changes in classical systems. A natural approach to modeling the dynamics of an open quantum system is to consider it as the result of an interaction between the system of interest and its surrounding environment [29]. Consequently, we assume that the quantum system in state $\rho = |\phi\rangle\langle\phi|$ interacts with the environment, so the final state of the system, $\mathcal{E}(\rho)$, may not be related to the initial state ρ by a unitary transformation.

Consider the input state as an arbitrary Bloch state vector, represented as follows:

$$|\phi_A\rangle = \cos\theta\ |0\rangle + e^{i\varphi} \sin\theta\ |1\rangle \tag{10}$$

where the angles $\theta \in [0, \pi]$ and $\varphi \in [0, 2\pi]$ correspond to rotations of the state vector around the y-axis and z-axis, respectively.

In the following, we outline the mathematical framework for noise analysis by considering two scenarios for noisy quantum systems: (1) when the quantum teleportation

process itself is affected by noise (Sec. 3.1) and (2) when the quantum channel is noisy (Sec. 3.2).

3.1 Impact of noise on quantum teleportation

In the first scenario, we analyze the quantum teleportation protocol under the influence of various noise types. For simplicity, we assume that all operations are affected by noise with equal probability, enabling a more tractable study of its impact on the transmitted quantum state. To examine the influence of noise, we adopt the framework of master equations, which provide a systematic approach for describing open quantum systems.

In particular, the master equation captures the continuous-time evolution of quantum noise through a differential equation governing the system's density matrix. The general Lindblad form is

$$\frac{\mathrm{d}\rho}{\mathrm{d}t} = -\frac{i}{\hbar}[H, \rho] + \sum_j \left(L_j \rho L_j^\dagger - \frac{1}{2} \left\{ L_j^\dagger L_j, \rho \right\} \right). \tag{11}$$

Here, $\{A, B\} = AB + BA$ denotes the anticommutator, H represents the system Hamiltonian that governs the coherent part of the dynamics, and L_j denotes the Lindblad operator encoding the system–environment interaction. Specifically, in the case of a two-level atomic system coupled to the vacuum, the Hamiltonian is given by $H = -\hbar\omega\sigma_z/2$, which corresponds to the coherent component of the atom's evolution.

The Lindblad operators corresponding to different types of noise are defined as follows:

- ***Bit-flip noise*** corresponds to the flipping of computational basis states. The associated Lindblad operator is given by $\sqrt{\gamma_{BF}}\,\sigma_x$, where γ_{BF} denotes the probability per unit time that a qubit state $|0\rangle$ flips to $|1\rangle$ (and vice versa).
- ***Phase-flip noise*** arises from a phase inversion of the quantum state, which induces errors in the encoded information. Its Lindblad operator is $\sqrt{\gamma_{PF}}\,\sigma_z$, with γ_{PF} representing the probability per unit time that the relative phase of the qubit state changes sign.
- ***Amplitude-damping noise*** describes the loss of energy from the system. It is characterized by the Lindblad operator $\sqrt{\gamma_{AD}}\,\sigma_-$, where $\sigma_- \equiv \frac{1}{2}(\sigma_x - i\sigma_y)$ and γ_{AD} denote the probability per unit time that an excited state $|1\rangle$ decays to the ground state $|0\rangle$.
- ***Phase-damping noise*** results from decoherence processes that affect the phase information of the quantum state due to environmental interactions. The corresponding Lindblad operator is $\sqrt{\gamma_{PD}}\,\sigma_\wedge$, where $\sigma_\wedge \equiv \frac{1}{2}(I - \sigma_z)$, and γ_{PD} denote the probability per unit time that quantum coherence (off-diagonal elements of the density matrix) is lost, while populations remain unchanged.

Quantum operations can be elegantly represented using the operator-sum representation, which explicitly expresses $\mathcal{E}(\rho)$ in terms of operators acting solely on the

Hilbert space of the principal system. Based on the solution presented in Appendix B, by employing the Lindblad operator together with the input density matrix, the operator $\mathcal{E}(\rho)$ can be expressed in the general operator-sum representation. Therefore, the operator-sum representation for a quantum system in state ρ after interacting with the environment can be written as follows [29]:

$$\mathcal{E}(\rho) = \sum_i \mathbf{E}_i \rho \mathbf{E}_i^\dagger, \qquad \mathbf{E}_i = E_i^{(1)} \otimes \cdots \otimes E_i^{(n)} \tag{12}$$

where E_i are operators on the state space of the principal system. The operators are referred to as the operation elements, or Kraus operators, for the quantum operation $\{\mathbf{E}_i\}$, which must satisfy the normalization condition $\sum_k E_k E_k^\dagger = I$.

In the first scenario, we analyze the influence of four different noise channels: 1. bit-flip (BF), 2. phase-flip (PF), 3. amplitude-damping (AD), and 4. phase-damping (PD). Hence, the operational elements for different types of quantum noise can be defined as follows [29] (see Appendix B):

$$E_0^{BF} = \sqrt{1 - p_{BF}}\, I, \quad E_1^{BF} = \sqrt{p_{BF}}\, \sigma_x \tag{13}$$

$$E_0^{PF} = \sqrt{1 - p_{PF}}\, I, \quad E_1^{PF} = \sqrt{p_{PF}}\, \sigma_z \tag{14}$$

$$E_0^{AD} = \begin{bmatrix} 1 & 0 \\ 0 & \sqrt{1 - p_{AD}} \end{bmatrix}, \quad E_1^{AD} = \sqrt{p_{AD}} \begin{bmatrix} 0 & 1 \\ 0 & 0 \end{bmatrix} \tag{15}$$

$$E_0^{PD} = \begin{bmatrix} 1 & 0 \\ 0 & \sqrt{1 - p_{PD}} \end{bmatrix}, \quad E_1^{PD} = \sqrt{p_{PD}} \begin{bmatrix} 0 & 0 \\ 0 & 1 \end{bmatrix} \tag{16}$$

where p represents the noise probabilities.

To examine the influence of noise on a quantum system during the teleportation process, we consider that every operation within the quantum controlled teleportation procedure U_{QCT} is affected by quantum noise with uniform sampling (see Fig. 4a).

In a multi-hop quantum communication scenario with m successive teleportation steps, this procedure must be repeated m times, resulting in the cumulative application of m noisy teleportation channels. Consequently, as the number of hops m increases, the quantum noise is expected to have a more pronounced detrimental effect on the fidelity of the final output state. In the discussion, we treat noise from teleportation operations as less significant than channel noise. Still, analyzing these effects is useful, since even with a lower probability, operational noise remains relevant compared to long-distance channel noise.

3.2 Characterization of noisy quantum channels

In the second scenario, we consider the case in which quantum noise acts directly on the quantum channel. Specifically, this implies that each GHZ state $\rho_{\text{GHZ}} = |\phi_{\text{GHZ}}\rangle\langle\phi_{\text{GHZ}}|$ within the channel is no longer in its ideal maximally entangled form. Based on the operator-sum representation and the specific type of noise, the noisy GHZ state can be modeled as shown in Eq. 11, corresponding to depolarizing and dephasing noise,

respectively [29].

$$\mathcal{E}_{\text{dep}}(\rho_{\text{GHZ}}) = (1 - p_{\text{dep}})\rho_{\text{GHZ}} + p_{\text{dep}} \cdot \frac{I^{\otimes n}}{2^n}, \tag{17}$$

and

$$\mathcal{E}_{\text{deph}}(\rho_{\text{GHZ}}) = (1 - p_{\text{dehp}})\rho_{\text{GHZ}} + \frac{p_{\text{deph}}}{2} \cdot (|0\rangle^{\otimes n}\langle 0|^{\otimes n} + |1\rangle^{\otimes n}\langle 1|^{\otimes n}) \tag{18}$$

where p_{dep} and p_{deph} represent the probabilities of noise effects for depolarizing and dephasing noise, respectively.

For analyzing the impact of noise in this case, it suffices to substitute each ideal GHZ state in quantum channel Eq. 5 with its noisy counterpart, effectively defining a noisy quantum channel. The teleportation process can then proceed as usual, following the subsequent steps outlined in the proposed protocol.

3.3 Quantitative analysis of noise effects

In quantum information theory, fidelity is a standard measure of the similarity between two quantum states [29]. It represents the likelihood that one state will be identified as another through an ideal measurement process. In this study, fidelity is employed as the primary metric to assess the effect of noise on the state transmitted through a noisy quantum system. Accordingly, the fidelity between the output state $\rho_f = |\psi_f\rangle\langle\psi_f|$ and the target (ideal) state $|\phi_A\rangle$ is defined as

$$F = \langle\phi_A|\rho_f|\phi_A\rangle, \tag{19}$$

where the fidelity value F ranges from 0 to 1. A fidelity value approaching 1 indicates a high degree of similarity between the two quantum states.

In Eq. 10, the input state $|\phi_A\rangle$ is considered to be an arbitrary pure state on the Bloch sphere. To generalize the analysis and evaluate the system's performance independently of a specific input, we introduce the concept of average fidelity F_{avg}. This allows us to study the behavior of the output state as a function of the noise intensity and its type. The average fidelity is defined in Eq. 20, where the integration over the input state parameters effectively reduces it to a function of the noise probability alone.

$$F_{avg} = \frac{1}{4\pi}\int_0^{2\pi}\int_0^{\pi} F(\phi_A, \rho_f)\sin\theta \, \mathrm{d}\theta\mathrm{d}\varphi \tag{20}$$

In both noisy system scenarios, it is expected that increasing the number of hops m, in conjunction with the noise probability, will lead to a notable decline in the fidelity of the transmitted quantum state. As shown in Figs. 4 and 5, the average fidelity decreases significantly across all noise types in both scenarios. This behavior is anticipated, as a greater number of hops corresponds to the cumulative application of noise, amplifying its overall impact on the quantum system.

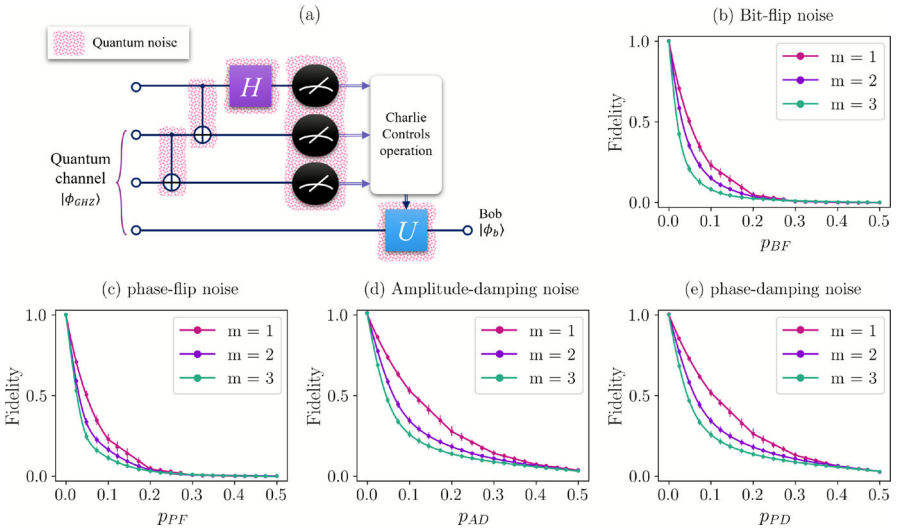

Fig. 4 **a** Quantum circuit representation of controlled quantum teleportation, highlighting the noisy regions. **b–e** Output state average fidelity of the m-hop quantum controlled teleportation protocol under different noise types on the teleportation process: **b** bit-flip noise; **c** phase-flip noise; **d** amplitude-damping noise; **e** phase-damping noise. The variable p represents the probability of noise

A comparison of the two scenarios—noisy quantum channels and noisy quantum teleportation—reveals that the latter imposes a more substantial degradation on the output state. This is primarily because, in the noisy teleportation scenario, noise is introduced at each step of the teleportation sequence, causing the quantum state to progressively deviate from its original form. In contrast, the noisy channel scenario transforms entangled GHZ states into mixed states; however, it does not directly perturb the initial input state. In the teleportation-based scenario, each hop introduces additional noise to the state already affected by the previous step, resulting in greater information loss as the state propagates through the system. However, quantum operations typically exhibit lower noise than quantum channels [10].

4 Simulation studies and experimental validation

To experimentally validate the proposed multi-hop quantum controlled teleportation protocol across varying numbers of hops, we implemented it using IBM's superconducting quantum hardware. Specifically, we utilized the 127-qubit quantum processor named `ibm_brisbane`, accessible via the IBM Quantum cloud platform [30]. This device is built upon a fixed-frequency transmon architecture arranged in a heavy-hex lattice configuration, as depicted in Fig. 6a. The processor features coherence times ranging from approximately 100 to 300 μs, with single- and two-qubit gate fidelities surpassing 99.9% and 99%, respectively, and a median readout error rate of roughly 1.7%.

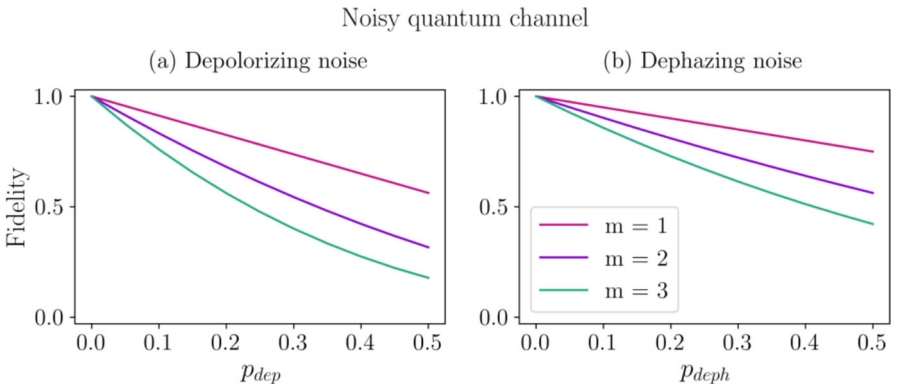

Fig. 5 Output state average fidelity of the multi-hop quantum controlled teleportation protocol under different noise types and hop counts. **a** Depolarizing noise on the quantum channel; **b** dephasing noise on the quantum channel. The variable p represents the probability of noise

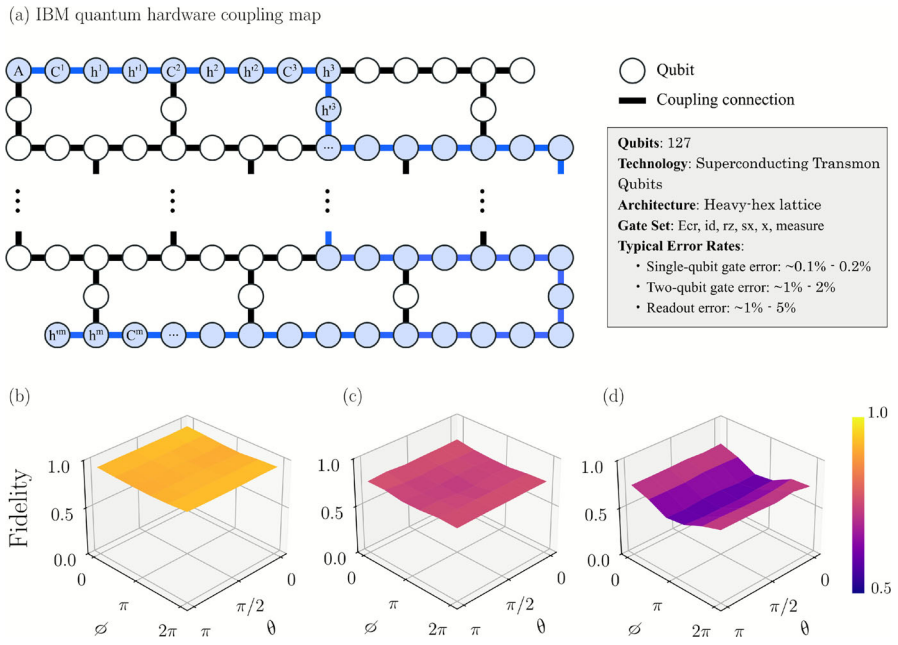

Fig. 6 **a** Schematic representation of the IBM quantum processor architecture (`ibm_brisbane`), highlighting its heavy-hex lattice structure and fixed-frequency transmon qubits. The proposed multi-hop quantum controlled teleportation protocol is mapped onto this hardware architecture. **b–d** Experimental results showing the fidelity of the teleported output state for different numbers of hops, **b** $m = 1$, **c** $m = 2$, and **d** $m = 3$. Each surface plot illustrates the fidelity as a function of the input state parameters $\theta \in [0, \pi]$ and $\varphi \in [0, 2\pi]$, demonstrating the degradation of fidelity with increasing number of hops

For benchmarking and validation, we also employed IBM's high-performance simulators, available through Qiskit [31]. These simulators incorporate detailed noise models that realistically capture the imperfections of actual IBM quantum devices, including gate infidelities, qubit connectivity constraints, measurement errors, and decoherence effects.

To enhance the quality of experimental results, we applied two error mitigation techniques: *twirled readout error extinction* (TREX) [32] and *dynamical decoupling* (DD) [33, 34]. TREX improves measurement accuracy by reducing readout errors through probabilistic averaging over symmetrized measurement outcomes [35]. DD, on the other hand, helps maintain quantum coherence during idle periods by applying tailored pulse sequences that dynamically refocus qubit states.

The experimental validation of the protocol included fidelity analysis of the output state for hop numbers $m = 1, 2$, and 3, using an arbitrary input state defined in Eq. 10. As illustrated in Fig. 6b–d, the input state parameters θ and φ were sampled across the full ranges $[0, \pi]$ and $[0, 2\pi]$, respectively, to assess the influence of the initial state on teleportation fidelity.

The results demonstrate a clear trend: as the number of hops increases, the fidelity between the output and target states degrades significantly. While the impact of the input parameters θ and φ is less discernible at lower hop counts, for larger m, a pronounced sensitivity emerges—particularly around $\varphi \approx \pi$, where the output fidelity shows increased susceptibility to system noise and operational errors.

5 Discussion and outlook

In the preceding sections, both numerical simulations and experimental observations demonstrated that increasing the number of hops in the teleportation process leads to a noticeable reduction in the fidelity of the teleported state. At first glance, this might suggest that multi-hop quantum networks offer no clear advantage over conventional single-link teleportation protocols. However, an important consideration must be made. In practice, the probability of noise within a quantum channel increases dramatically with the physical distance of transmission. Consequently, when teleportation is performed over very long distances through a direct channel, the fidelity of the transmitted state deteriorates far more severely than in a multi-hop configuration. In the following discussion, we highlight how multi-hop protocols can, despite their local fidelity losses at each hop, provide a significant advantage in maintaining higher overall fidelity for long-distance quantum teleportation.

In long-distance quantum communication, attenuation and environmental disturbances during transmission play a crucial role in shaping the channel's noise characteristics. Accordingly, two fundamental models of noise are typically employed to describe quantum channels: dephasing noise and depolarizing noise.

For optical fiber links, the channel transmissivity decreases exponentially with the transmission distance D, expressed as

$$\eta(D) = 10^{-\alpha D/10}, \tag{21}$$

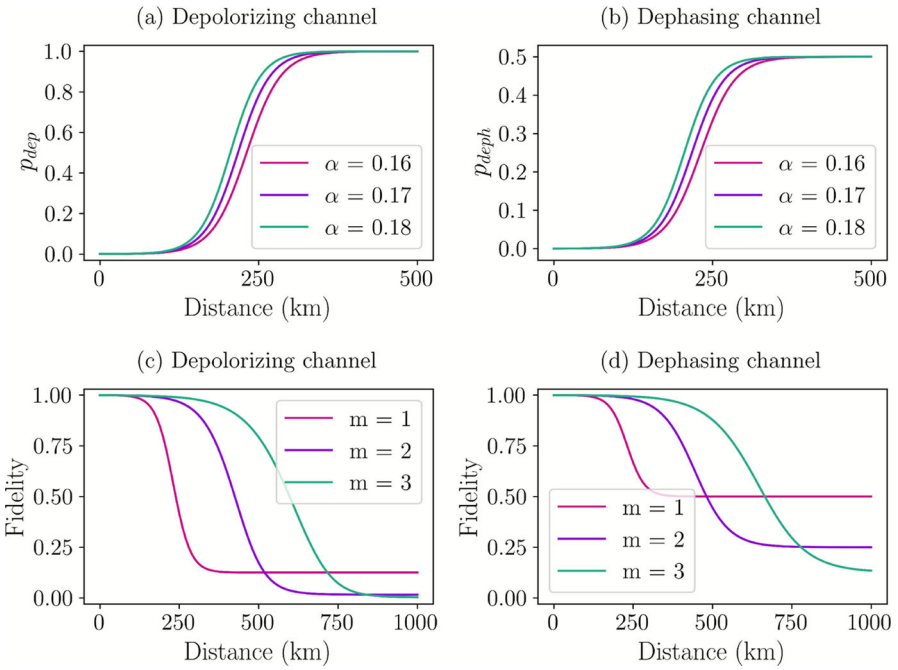

Fig. 7 Noise probability versus transmission distance (km) in quantum channels for attenuation coefficients $\alpha = 0.16, 0.17$, and 0.18 for **a** depolarizing and **b** dephasing channels. Output state average fidelity versus distance (km) for hop numbers $m = 1, 2$, and 3 for **c** depolarizing and **d** dephasing channels

where α (dB/km) is the attenuation coefficient and D denotes the fiber length [2]. As the distance increases, the relative impact of background contributions and detector dark counts grows compared to the photon flux, thereby enhancing the effective noise probability per detection event. The interference visibility observed in the system can be modeled as

$$V(D) = \frac{S_0 \eta(D)}{S_0 \eta(D) + N}, \tag{22}$$

where S_0 is the zero-distance signal rate and N represents a distance-independent noise term. Consequently, the noise probability associated with detection in an optical link can be expressed in terms of visibility as $p_{\text{noise}} = f(V(D))$. This relation has been extensively applied in entanglement distribution and teleportation experiments across long distances [36, 37].

From the perspective of a quantum channel, the visibility can be directly mapped onto the noise parameters of standard channel models. Specifically, the depolarizing noise probability is given by $p_{\text{dep}} = 1 - V(D)$, while the dephasing noise probability is expressed as $p_{\text{deph}} = \frac{1-V(D)}{2}$ [29]. Figure 7 illustrates the dependence of the noise probability on the quantum channel distance for two distinct types of noise.

In the preceding section, the noise analysis of the quantum channel (Fig. 6) revealed that the fidelity of the proposed multi-hop protocol decreases significantly as the number of hops increases. However, examining the relationship between channel noise

and distance, as illustrated in Fig. 7, offers an important complementary viewpoint. For instance, consider the task of teleporting a quantum state over a distance of $D \approx 300$ km. As shown in Fig. 7a, b, the noise probability approaches its maximum for such long-distance channels, which, according to Fig. 6, reduces the protocol fidelity to below 0.5—the threshold corresponding to a classical guess. In contrast, if the proposed protocol is implemented with $m = 3$ hops, the total distance is divided into three segments of approximately 100 km each. At $D' \approx 100$ km, Fig. 7a, b indicates that the noise probability is nearly zero, yielding an almost ideal fidelity in the corresponding noise analysis, as depicted in Fig. 7c, d.

Although practical systems will not achieve such ideal performance, this example highlights the fundamental advantage of quantum repeaters in suppressing channel-induced errors [10, 38]. In realistic settings, however, numerous additional parameters must be considered when designing the optimal structure of a quantum communication network, which makes the problem inherently a trade-off. To illustrate the trade-off between the number of hops and the fidelity of the transmitted quantum state, we assume that the noise probability per hop can be approximated as a linear combination of channel noise and operation noise, denoted by p_{ch} and p_{op}, respectively:

$$p_{hop} \approx p_{ch} + p_{op}. \tag{23}$$

Since the operation noise is independent of transmission distance, we set it to zero for this analysis. In this case, the channel noise probability can be described as a combination of two types of quantum noise—depolarizing and dephasing—that simultaneously affect the channel:

$$p_{ch} = \begin{cases} 1 - V(D), & \text{depolarizing noise,} \\ \frac{1}{2}\big(1 - V(D)\big), & \text{dephasing noise.} \end{cases} \tag{24}$$

According to the generalized MQCT protocol, the required quantum and classical resources per hop are $Q = 3nm$ qubits and $C = 2nm$ bits, respectively. By defining the output state average fidelity as a function of distance and hop count, $F_{av}(D, m)$, the optimal network configuration must satisfy the following constraints:

$$F_{av}(D, m) \geq F_{min}, \qquad Q \leq Q_{max}, \qquad C \leq C_{max}, \tag{25}$$

where F_{min}, Q_{max}, and C_{max} represent the fidelity and resource constraints imposed by the network.

A simple approach to determine the optimal number of hops is to introduce a cost function defined over these parameters:

$$\text{cost} = -F_{avg} + \lambda_Q Q + \lambda_C C, \tag{26}$$

where λ_Q and λ_C are weighting parameters that reflect the relative importance of different resource types. The optimal hop count m^* is then obtained by minimizing

the cost function:

$$m^* = \arg\min_{m \in \mathbb{N}} \text{cost} . \tag{27}$$

Our numerical and experimental investigations reveal a clear trade-off between the number of hops and the resulting fidelity of the transmitted quantum state. While multi-hop controlled teleportation extends communication distance, each additional hop introduces accumulated noise and decoherence, ultimately degrading the final fidelity. The experimental implementation of the proposed protocol demonstrates its practicality on current hardware and underscores the need to incorporate post-processing techniques to ensure reliable state transfer. These findings further emphasize the importance of evaluating quantum performance metrics alongside classical network design parameters, particularly when balancing communication distance, resource expenditure, and noise sensitivity in quantum communication systems.

This study contributes to narrowing the gap between theoretical models and experimental realizations by presenting one of the few empirical assessments of multi-hop quantum teleportation under realistic noise conditions. Beyond hardware advancements, several theoretical and experimental strategies can be employed to improve fidelity. Error mitigation techniques can reduce noise at each hop, quantum error correction can reinforce the teleportation process, and entanglement purification (or distillation) [39] can be used to establish higher-quality quantum channels. Integrating these methods with improvements in device-level performance—such as longer coherence times, higher gate fidelities, and lower readout errors—will be essential for enabling reliable long-distance quantum networks [38].

6 Conclusion

In this study, we proposed a generalized protocol for multi-hop quantum controlled teleportation, explicitly accounting for the effects of different types and levels of quantum noise. The reliable transmission of quantum information over long distances remains a central challenge in quantum communication. Developments such as quantum repeaters and multi-hop quantum networks have enabled improvements in the fidelity and robustness of quantum teleportation over noisy channels.

Our protocol addresses the trade-off between resource efficiency and noise impact, enabling the construction of flexible multi-hop quantum networks based on system constraints. The protocol was experimentally validated on the IBM quantum platform, enabling us to evaluate its practical performance on a real quantum device.

Furthermore, we analyzed the influence of different common types of quantum noise on the performance of the protocol. This analysis enhanced the interpretability of our approach under realistic noise conditions. The results demonstrated that performing noisy quantum teleportation at each hop results in cumulative degradation of the output state's fidelity, making it increasingly vulnerable to noise as the number of hops increases.

However, our findings also highlight the potential of post-processing techniques—such as quantum error correction, error mitigation, and entanglement distillation—to significantly reduce the adverse effects of noise. By applying these methods, it is pos-

sible to maintain acceptable fidelity levels even in multi-hop scenarios. Experimental results incorporating error mitigation techniques further confirmed the effectiveness of post-processing in improving the final output state.

Appendix A Multi-hop quantum controlled teleportation

A.1 Single-hop QCT protocol

In a single-hop QCT, Alice intends to transmit a quantum state $|\phi_A\rangle$ to Bob via a single-hop quantum channel. The quantum state prepared by Alice is given as:

$$|\phi_A\rangle = \alpha_0|0\rangle + \alpha_1|1\rangle \tag{A1}$$

subject to the normalization condition $\sum_i |\alpha_i|^2 = 1$, which ensures the state is properly normalized.

The initial state of the composite quantum system can be expressed as:

$$|\psi_0\rangle = |\phi_A\rangle \otimes |\phi_{ch}\rangle \tag{A2}$$

In this expression, $|\phi_{ch}\rangle$ represents the entangled quantum channel, which involves Charlie and the qubits corresponding to the first hop, denoted by $|\phi_h\rangle$ and $|\phi_{h'}\rangle$. The shared quantum channel is assumed to be a GHZ state, defined as:

$$|\phi_{ch}\rangle = |\phi_C\rangle \otimes |\phi_{hh'}\rangle = \frac{1}{\sqrt{2}}(|000\rangle + |111\rangle)_{Chh'} \tag{A3}$$

For clarity and to facilitate subsequent analysis, the GHZ state given in Eq. A2 can be equivalently reformulated in an extended form as:

$$\begin{aligned} |\psi_0\rangle =& (\alpha_0|0\rangle + \alpha_1|1\rangle)_A \otimes (\frac{1}{\sqrt{2}}(|000\rangle + |111\rangle))_{Chh'} \\ =& \frac{1}{\sqrt{2}}(\alpha_0|0000\rangle + \alpha_0|0111\rangle + \alpha_1|1000\rangle + \alpha_1|1111\rangle)_{AChh'}. \end{aligned} \tag{A4}$$

In the single-hop QCT, only one teleportation process is performed. Consequently, in the first step, qubits $|\phi_A\rangle$, $|\phi_C\rangle$, and $|\phi_h\rangle$ must be transformed into the GHZ basis. To achieve this, a unitary operation U_1 is applied to these qubits as follows:

$$\begin{aligned} |\psi_1\rangle =& \frac{1}{\sqrt{2}}(U_1 \otimes I)(\alpha_0|0000\rangle + \alpha_0|0111\rangle + \alpha_1|1000\rangle + \alpha_1|1111\rangle)_{AChh'} \\ =& \frac{1}{2}(\alpha_0|0000\rangle + \alpha_0|1000\rangle + \alpha_0|0101\rangle + \alpha_0|1101\rangle \\ & + \alpha_1|0100\rangle - \alpha_1|1100\rangle + \alpha_1|0001\rangle - \alpha_1|1001\rangle)_{AChh'}, \end{aligned} \tag{A5}$$

where the operator U_1 corresponds to the inverse GHZ operation, denoted as $U_{\text{GHZ}}^{\dagger}$.

Table 1 Required correction operators for reconstructing the shared quantum state based on measurement outcomes in the quantum controlled teleportation (QCT) protocol

Measurement outcome of $\|\phi_A\rangle$	Measurement outcome of $\|\phi_h\rangle$	Measurement outcome of $\|\phi_C\rangle$	Required Operator
0	0	0	I
0	0	1	X
0	1	0	Invalid[1]
0	1	1	Invalid
1	0	0	Z
1	0	1	ZX
1	1	0	Invalid
1	1	1	Invalid

[1]Entries marked as "Invalid" indicate measurement outcomes excluded due to protocol errors

In the second step, qubits $|\phi_A\rangle$, $|\phi_C\rangle$, and $|\phi_h\rangle$ are measured, and the measurement outcome, represented by $k \in \{0, 1\}$, is obtained according to:

$$|\psi_{1k}\rangle = \frac{M_k|\psi_1\rangle}{\sqrt{\langle\psi_1|M_k^\dagger M_k|\psi_1\rangle}} \tag{A6}$$

Based on the measurement results and following the correction operations specified in Table 1, the appropriate unitary transformations are applied to qubit $|\phi_{h'}\rangle$ in order to reconstruct the original input state at the output. The corresponding quantum state of the system can be expressed as:

$$\begin{aligned}|\psi_2\rangle = \frac{1}{2}(&\alpha_0(M_{ACh}\otimes I)|0000\rangle + \alpha_0(M_{ACh}\otimes \ \ Z)|1000\rangle\\ &+\alpha_0(M_{ACh}\otimes X)|0101\rangle + \alpha_0(M_{ACh}\otimes ZX)|1101\rangle\\ &+\alpha_1(M_{ACh}\otimes X)|0100\rangle - \alpha_1(M_{ACh}\otimes ZX)|1100\rangle\\ &+\alpha_1(M_{ACh}\otimes \ I)|0001\rangle - \alpha_1(M_{ACh}\otimes \ \ Z)|1001\rangle)_{AChh'}\end{aligned} \tag{A7}$$

where M_{ACh} means measurement over $|\phi_A\rangle$, $|\phi_C\rangle$, and $|\phi_h\rangle$ states.

Finally, considering the normalization condition, the final teleported state of the quantum system is given by:

$$\begin{aligned}|\psi_f\rangle =& \frac{1}{2}\frac{(4\alpha_0|0\rangle + 4\alpha_1|1\rangle)}{2}\\ =& \alpha_0|0\rangle + \alpha_1|1\rangle\end{aligned} \tag{A8}$$

A.2 Two-hop protocol

In the two-hop QCT, the quantum system utilizes two GHZ states as the quantum channel, which can be represented as:

$$|\phi_{ch}\rangle = |\phi_{C^1h^1h'^1}\rangle \otimes |\phi_{C^2h^2h'^2}\rangle = \frac{1}{\sqrt{2}}(|000\rangle + |111\rangle)_{C^1h^1h'^1} \otimes \frac{1}{\sqrt{2}}(|000\rangle + |111\rangle)_{C^2h^2h'^2} \tag{A9}$$

As in the single-hop protocol, Alice aims to transmit the quantum state defined in Eq. A1 through the quantum channel described by Eq. A9. Consequently, the initial state of the entire quantum system is expressed as:

$$\begin{aligned}|\psi_0\rangle =&(\alpha_0|0\rangle + \alpha_1|1\rangle)_A \otimes \frac{1}{\sqrt{2}}(|000\rangle + |111\rangle)_{C^1h^1h'^1} \\ &\otimes \frac{1}{\sqrt{2}}(|000\rangle + |111\rangle)_{C^2h^2h'^2} \\ =&\frac{1}{2}(\alpha_0|0000000\rangle + \alpha_0|0000111\rangle + \alpha_0|0111000\rangle + \alpha_0|0111111\rangle \\ &+ \alpha_1|1000000\rangle + \alpha_1|1000111\rangle + \alpha_1|1111000\rangle \\ &+ \alpha_1|1111111\rangle)_{AC^1h^1h'^1C^2h^2h'^2}\end{aligned} \tag{A10}$$

In the first step, the unitary operator U_1 is applied to qubits $|\phi_A\rangle$, $|\phi_{C^1}\rangle$, and $|\phi_{h^1}\rangle$ in order to prepare the system for measurement in the GHZ basis:

$$\begin{aligned}|\psi_1\rangle =&\frac{1}{2}(U_1 \otimes I^{\otimes 3})(\alpha_0|0000000\rangle + \alpha_0|0000111\rangle \\ &+ \alpha_0|0111000\rangle + \alpha_0|0111111\rangle \\ &+ \alpha_1|1000000\rangle + \alpha_1|1000111\rangle + \alpha_1|1111000\rangle \\ &+ \alpha_1|1111111\rangle)_{AC^1h^1h'^1C^2h^2h'^2} \\ =&\frac{1}{2\sqrt{2}}(\alpha_0|+000000\rangle + \alpha_0|+000111\rangle + \alpha_0|+101000\rangle \\ &+ \alpha_0|+101111\rangle \\ &+ \alpha_1|-100000\rangle + \alpha_1|-100111\rangle + \alpha_1|-001000\rangle \\ &+ \alpha_1|-001111\rangle)_{AC^1h^1h'^1C^2h^2h'^2}\end{aligned} \tag{A11}$$

where the operator U_1 corresponds to the inverse GHZ operation, denoted as $U^{\dagger}_{\text{GHZ}}$.

Based on the measurement outcomes of qubits $|\phi_A\rangle$, $|\phi_{C^1}\rangle$, and $|\phi_{h^1}\rangle$, appropriate correction operators—determined by Table 1—are applied to qubit $|\phi_{h'^1}\rangle$. The

quantum system then evolves to the following state:

$$\begin{aligned}|\psi_2\rangle = \frac{1}{4}(&\alpha_0(I\otimes I^{\otimes 3})|0000\rangle + \alpha_0(Z\otimes I^{\otimes 3})|0000\rangle\\ &+\alpha_0(I\otimes I^{\otimes 3})|0111\rangle + \alpha_0(Z\otimes I^{\otimes 3})|0111\rangle\\ &+\alpha_0(X\otimes I^{\otimes 3})|1000\rangle + \alpha_0(ZX\otimes I^{\otimes 3})|1000\rangle\\ &+\alpha_0(X\otimes I^{\otimes 3})|1111\rangle + \alpha_0(ZX\otimes I^{\otimes 3})|1111\rangle\\ &+\alpha_1(X\otimes I^{\otimes 3})|0000\rangle - \alpha_1(ZX\otimes I^{\otimes 3})|0000\rangle\\ &+\alpha_1(X\otimes I^{\otimes 3})|0111\rangle - \alpha_1(ZX\otimes I^{\otimes 3})|0111\rangle\\ &+\alpha_1(I\otimes I^{\otimes 3})|1000\rangle - \alpha_1(I\otimes Z^{\otimes 3})|1000\rangle\\ &+\alpha_1(I\otimes I^{\otimes 3})|1111\rangle - \alpha_1(Z\otimes I^{\otimes 3})|1111\rangle)_{h'^1C^2h^2h'^2}\end{aligned} \tag{A12}$$

This state can be equivalently rewritten as:

$$|\psi_3\rangle = \frac{1}{2}(\alpha_0|0000\rangle + \alpha_0|0111\rangle + \alpha_1|1000\rangle + \alpha_1|1111\rangle)_{h'^1C^2h^2h'^2} \tag{A13}$$

Subsequently, a second unitary operation U_2 is applied to qubits $|\phi_{h'^1}\rangle$, $|\phi_{C^2}\rangle$, and $|\phi_{h^2}\rangle$ to prepare them for GHZ measurement. The quantum system is then transformed into:

$$\begin{aligned}|\psi_4\rangle =&\frac{1}{\sqrt{2}}(U_2\otimes I)(\alpha_0|0000\rangle + \alpha_0|0111\rangle + \alpha_1|1000\rangle + \alpha_1|1111\rangle)_{h'^1C^2h^2h'^2}\\ =&\frac{1}{\sqrt{2}}(\alpha_0|0000\rangle + \alpha_0|1000\rangle + \alpha_0|0101\rangle + \alpha_0|1101\rangle\\ &+\alpha_1|0100\rangle - \alpha_1|1100\rangle + \alpha_1|0001\rangle - \alpha_1|1001\rangle)_{h'^1C^2h^2h'^2}\end{aligned} \tag{A14}$$

where the operator U_2 corresponds to the inverse GHZ operation, denoted as $U^{\dagger}_{\mathrm{GHZ}}$.

Finally, using the correction operators specified in Table 1, suitable operations are applied to qubit $|\phi_{h'^2}\rangle$ based on the measurement outcomes of qubits $|\phi_{h'^1}\rangle$, $|\phi_{C^2}\rangle$, and $|\phi_{h^2}\rangle$. The resulting quantum system state can be written as:

$$\begin{aligned}|\psi_5\rangle = \frac{1}{\sqrt{2}}(&\alpha_0 I|0\rangle + \alpha_0 Z|0\rangle + \alpha_0 X|1\rangle + \alpha_0 ZX|1\rangle\\ &+\alpha_1 X|0\rangle - \alpha_1 ZX|0\rangle + \alpha_1 I|1\rangle - \alpha_1 Z|1\rangle)_{h'^2}\end{aligned} \tag{A15}$$

This final state can also be expressed in the following equivalent form:

$$\begin{aligned}|\psi_6\rangle =&\frac{1}{\sqrt{2}}\frac{(4\alpha_0|0\rangle + 4\alpha_1|1\rangle)}{2\sqrt{2}}\\ =&\alpha_0|0\rangle + \alpha_1|1\rangle\end{aligned} \tag{A16}$$

Appendix B Quantum noise representation

To solve the Lindblad master equation Eq. 11, it is helpful to move the interaction picture to make change of variables

$$\bar{\rho}(t) \equiv e^{iHt}\rho(t)e^{-iHt}, \tag{B17}$$

where the $\bar{\rho}(t)$ can be represent in density matrix representation as follows,

$$\bar{\rho}(t) = \begin{bmatrix} \rho_{00}(t) & \rho_{01}(t) \\ \rho_{10}(t) & \rho_{11}(t) \end{bmatrix} \tag{B18}$$

Hence, in the next step we only need to solve the Lindblas equation in Eq. 11 using density matrix representation in Eq. B18 for different noise types (corresponding Lindblad operators).

B.1 Bit-flip noise

Considering the Lindblad operator $L_j = \sqrt{\gamma_{BF}}\sigma_x$ for the bit-flip noise, the corresponding master equation Eq. 11 can be written as

$$\begin{aligned} \frac{\mathrm{d}\bar{\rho}}{\mathrm{d}t} &= \gamma_{BF}\left(\sigma_x\bar{\rho}\sigma_x^\dagger - \frac{1}{2}\sigma_x^\dagger\sigma_x\bar{\rho} - \frac{1}{2}\bar{\rho}\sigma_x^\dagger\sigma_x\right) \\ &= \gamma_{BF}\left(\sigma_x\bar{\rho}\sigma_x - \bar{\rho}\right), \end{aligned} \tag{B19}$$

where $\sigma_x \equiv \sigma_x^\dagger$ denotes the Pauli-X operator.
Solving Eq. B19 for the density matrix elements (Eq. B18) yields

$$\begin{aligned} \bar{\rho}_{00}(t) =& \frac{1}{2}\Big(\bar{\rho}_{00}(0) + \bar{\rho}_{11}(0) + (\bar{\rho}_{00}(0) - \bar{\rho}_{11}(0))e^{-\gamma_{BF}t}\Big), \\ \bar{\rho}_{01}(t) =& \Re[\bar{\rho}_{01}(0)] + i\,\Im[\bar{\rho}_{01}(0)]e^{-\gamma_{BF}t}, \\ \bar{\rho}_{10}(t) =& \Re[\bar{\rho}_{01}(0)] - i\,\Im[\bar{\rho}_{01}(0)]e^{-\gamma_{BF}t}, \\ \bar{\rho}_{11}(t) =& \frac{1}{2}\Big(\bar{\rho}_{00}(0) + \bar{\rho}_{11}(0) - (\bar{\rho}_{00}(0) - \bar{\rho}_{11}(0))e^{-\gamma_{BF}t}\Big). \end{aligned} \tag{B20}$$

Thus, the density matrix can be expressed as

$$\bar{\rho}(t) = \begin{bmatrix} \frac{1}{2}(\bar{\rho}_{00}(0) + \bar{\rho}_{11}(0) + (\bar{\rho}_{00}(0) - \bar{\rho}_{11}(0))e^{-\gamma_{BF}t}) & \Re[\bar{\rho}_{01}(0)] + i\,\Im[\bar{\rho}_{01}(0)]e^{-\gamma_{BF}t} \\ \Re[\bar{\rho}_{01}(0)] - i\,\Im[\bar{\rho}_{01}(0)]e^{-\gamma_{BF}t} & \frac{1}{2}(\bar{\rho}_{00}(0) + \bar{\rho}_{11}(0) - (\bar{\rho}_{00}(0) - \bar{\rho}_{11}(0))e^{-\gamma_{BF}t}) \end{bmatrix}. \tag{B21}$$

Introducing the noise probability $p_{BF} \approx \frac{1}{2}(1 - e^{-\gamma_{BF}t})$, the density matrix takes the form

$$\bar{\rho}(t) = \begin{bmatrix} (1-p_{BF})\bar{\rho}_{00}(0) + p_{BF}\bar{\rho}_{11}(0) & (1-p_{BF})\bar{\rho}_{01}(0) + p_{BF}\bar{\rho}_{10}(0) \\ (1-p_{BF})\bar{\rho}_{10}(0) + p_{BF}\bar{\rho}_{01}(0) & (1-p_{BF})\bar{\rho}_{11}(0) + p_{BF}\bar{\rho}_{00}(0) \end{bmatrix}. \quad \text{(B22)}$$

Finally, the channel can be expressed in operator-sum (Kraus) form as

$$\bar{\rho}(t) = \mathcal{E}(\bar{\rho}(0)) \equiv I\bar{\rho}(0)I^\dagger + X\bar{\rho}(0)X^\dagger, \quad \text{(B23)}$$

which corresponds to the Kraus representation of the bit-flip noise (Eq. 13).

B.2 Phase-flip noise

Considering the Lindblad operator $L_j = \sqrt{\gamma_{PF}}\sigma_z$ for the phase-flip noise, the corresponding master equation Eq. 11 can be written as

$$\begin{aligned} \frac{\mathrm{d}\bar{\rho}}{\mathrm{d}t} &= \gamma_{PF}\left(\sigma_z\bar{\rho}\sigma_z^\dagger - \frac{1}{2}\sigma_z^\dagger\sigma_z\bar{\rho} - \frac{1}{2}\rho\sigma_z^\dagger\sigma_z\right) \\ &= \gamma_{PF}\left(\sigma_z\bar{\rho}\sigma_z - \bar{\rho}\right) \end{aligned} \quad \text{(B24)}$$

where $\sigma_z \equiv \sigma_z^\dagger$ denotes the Pauli-Z operator.

Solving Eq. B24 for the density matrix elements (Eq. B19) yields

$$\begin{aligned} \bar{\rho}_{00}(t) &= \bar{\rho}_{00}(0) \\ \bar{\rho}_{01}(t) &= \bar{\rho}_{01}(0)e^{-\gamma_{PF}t} \\ \bar{\rho}_{10}(t) &= \bar{\rho}_{10}(0)e^{-\gamma_{PF}t} \\ \bar{\rho}_{11}(t) &= \bar{\rho}_{11}(0) \end{aligned} \quad \text{(B25)}$$

Thus, the density matrix can be expressed as

$$\bar{\rho}(t) = \begin{bmatrix} \bar{\rho}_{00}(0) & \bar{\rho}_{01}(0)e^{-\gamma_{PF}t} \\ \bar{\rho}_{10}(0)e^{-\gamma_{PF}t} & \bar{\rho}_{11}(0) \end{bmatrix} \quad \text{(B26)}$$

Introducing the noise probability $p_{PF} \approx \frac{1}{2}(1 - e^{-\gamma_{PF}t})$, the density matrix takes the form

$$\bar{\rho}(t) = \begin{bmatrix} \bar{\rho}_{00}(0) & (1-2p_{PF})\bar{\rho}_{01}(0) \\ (1-2p_{PF})\bar{\rho}_{10}(0) & \bar{\rho}_{11}(0) \end{bmatrix} \quad \text{(B27)}$$

Finally, the channel can be expressed in operator-sum (Kraus) form as

$$\bar{\rho}(t) = \mathcal{E}(\bar{\rho}(0)) \equiv I\bar{\rho}(0)I^\dagger + Z\bar{\rho}(0)Z^\dagger \quad \text{(B28)}$$

which corresponds to the Kraus representation of the phase-flip noise (Eq. 14).

B.3 Amplitude-damping noise

Considering the Lindblad operator $L_j = \sqrt{\gamma_{AD}}\sigma_+$ for the amplitude-damping noise, the corresponding master equation Eq. 11 can be written as

$$\frac{\mathrm{d}\bar{\rho}}{\mathrm{d}t} = \gamma_{AD}\left(\sigma_-\bar{\rho}\sigma_+ - \frac{1}{2}\sigma_+\sigma_-\bar{\rho} - \frac{1}{2}\rho\sigma_+\sigma_-\right), \tag{B29}$$

where $\sigma_+ \equiv \sigma_-^\dagger$ represents the atomic raising operator.

Solving Eq. B29 for the density matrix elements (Eq. B19) yields

$$\begin{aligned}
\bar{\rho}_{00}(t) =& 1 - \bar{\rho}_{11}(t)\\
\bar{\rho}_{01}(t) =& \bar{\rho}_{01}(0)e^{-\gamma_{AD}t/2}\\
\bar{\rho}_{10}(t) =& \bar{\rho}_{10}(0)e^{-\gamma_{AD}t/2}\\
\bar{\rho}_{11}(t) =& \bar{\rho}_{11}(0)e^{-\gamma_{AD}t}
\end{aligned} \tag{B30}$$

Thus, the density matrix can be expressed as

$$\bar{\rho}(t) = \begin{bmatrix} 1 - \bar{\rho}_{11}(0)e^{-\gamma_{AD}t} & \bar{\rho}_{01}(0)e^{-\gamma_{AD}t/2} \\ \bar{\rho}_{10}(0)e^{-\gamma_{AD}t/2} & \bar{\rho}_{11}(0)e^{-\gamma_{AD}t} \end{bmatrix} \tag{B31}$$

Introducing the noise probability $p_{AD} = 1 - e^{-2\gamma_{AD}t} \approx 1 - e^{-t/T_1}$ (T_1 is energy relaxation time), the density matrix takes the form

$$\bar{\rho}(t) = \begin{bmatrix} \bar{\rho}_{00}(0) + p_{AD}\bar{\rho}_{11}(0) & \sqrt{1 - p_{AD}}\bar{\rho}_{01}(0) \\ \sqrt{1 - p_{AD}}\bar{\rho}_{10}(0) & (1 - p_{AD})\bar{\rho}_{11}(0) \end{bmatrix} \tag{B32}$$

Finally, the channel can be expressed in operator-sum (Kraus) form as

$$\bar{\rho}(t) = \mathcal{E}(\bar{\rho}(0)) \equiv E_0^{AD}\bar{\rho}(0)E_0^{AD^\dagger} + E_1^{AD}\bar{\rho}(0)E_1^{AD^\dagger} \tag{B33}$$

which corresponds to the Kraus representation of the amplitude-damping noise (Eq. 15).

B.4 Phase-damping noise

Considering the Lindblad operator $L_j = \sqrt{\gamma_{PD}}\sigma_\wedge$ for the phase-damping noise, the corresponding master equation Eq. 11 can be written as

$$\frac{\mathrm{d}\bar{\rho}}{\mathrm{d}t} = \gamma_{PD}\left(\sigma_\wedge\bar{\rho}\sigma_\wedge^\dagger - \frac{1}{2}\sigma_\wedge^\dagger\sigma_\wedge\bar{\rho} - \frac{1}{2}\rho\sigma_\wedge^\dagger\sigma_\wedge\right) \tag{B34}$$

where $\sigma_\wedge \equiv \sigma_\wedge^\dagger$.

Solving Eq. B34 for the density matrix elements (Eq. B19) yields

$$\begin{aligned}\bar{\rho}_{00}(t) &= \bar{\rho}_{11}(0)\\ \bar{\rho}_{01}(t) &= \bar{\rho}_{01}(0)e^{-\gamma_{PD}t}\\ \bar{\rho}_{10}(t) &= \bar{\rho}_{10}(0)e^{-\gamma_{PD}t}\\ \bar{\rho}_{11}(t) &= \bar{\rho}_{11}(0)\end{aligned} \tag{B35}$$

Thus, the density matrix can be expressed as

$$\bar{\rho}(t) = \begin{bmatrix} \bar{\rho}_{00}(0) & \bar{\rho}_{01}(0)e^{-\gamma_{PD}t} \\ \bar{\rho}_{10}(0)e^{-\gamma_{PD}t} & \bar{\rho}_{11}(0) \end{bmatrix} \tag{B36}$$

In quantum system, the pure dephasing time T_ϕ satisfies the following expression

$$\frac{1}{T_2} = \frac{1}{2T_1} + \frac{1}{T_\phi} \tag{B37}$$

where T_1 and T_2 are energy relaxation time and dephasing time, respectively.

Introducing the noise probability $p_{PD} = 1 - e^{-t/T_\phi}$, the density matrix takes the form

$$\bar{\rho}(t) = \begin{bmatrix} \bar{\rho}_{00}(0) & (1-p_{PD})\bar{\rho}_{01}(0) \\ (1-p_{PD})\bar{\rho}_{10}(0) & \bar{\rho}_{11}(0) \end{bmatrix} \tag{B38}$$

Finally, the channel can be expressed in operator-sum (Kraus) form as

$$\bar{\rho}(t) = \mathcal{E}(\bar{\rho}(0)) \equiv E_0^{PD}\bar{\rho}(0)E_0^{PD\dagger} + E_1^{PD}\bar{\rho}(0)E_1^{PD\dagger} \tag{B39}$$

which corresponds to the Kraus representation of the phase-damping noise (Eq. 16).

Acknowledgements No acknowledgments.

Author Contributions M.M.F. was responsible for formulating the research concept, developing the numerical solutions, conducting the literature review, and drafting the manuscript. Y.M. contributed to the literature review, manuscript preparation, data visualization, and implementation of the computational code.

Funding Open access funding provided by Tampere University (including Tampere University Hospital).

Data Availability No datasets were generated or analyzed during the current study.

Declarations

Conflict of interest The authors declare no conflict of interest.

Ethical approval The authors ethically approve the material of the paper. The authors have been informed of the consent regarding the submission of the article. No human/animal has participated in this research.

References

1. Gisin, N., Thew, R.: Quantum communication. Nat. Photon. **1**(3), 165–171 (2007). https://doi.org/10.1038/nphoton.2007.22
2. Wehner, S., Elkouss, D., Hanson, R.: Quantum internet: a vision for the road ahead. Science **362**(6412), 9288 (2018). https://doi.org/10.1126/science.aam9288
3. Gyongyosi, L., Imre, S.: Scalable distributed gate-model quantum computers. Sci. Rep. **11**(1), 5172 (2021). https://doi.org/10.1038/s41598-020-76728-5
4. Gyongyosi, L.: Adaptive problem solving dynamics in gate-model quantum computers. Entropy **24**(9), 1196 (2022). https://doi.org/10.3390/e24091196
5. Gyongyosi, L., Imre, S.: Circuit depth reduction for gate-model quantum computers. Sci. Rep. **10**(1), 11229 (2020). https://doi.org/10.1038/s41598-020-67014-5
6. Gyongyosi, L., Imre, S.: Networked quantum services. Quantum Inf. Comput. **25**(2025), 97–140 (2025). https://doi.org/10.2478/qic-2025-0006
7. Gyongyosi, L., Imre, S.: Advances in the quantum internet. Commun. ACM **65**(8), 52–63 (2022). https://doi.org/10.1145/3524455
8. Gyongyosi, L., Imre, S., Nguyen, H.V.: A survey on quantum channel capacities. IEEE Commun. Surv. Tutor. **20**(2), 1149–1205 (2018). https://doi.org/10.1109/COMST.2017.2786748
9. Bennett, C.H., Brassard, G., Crépeau, C., Jozsa, R., Peres, A., Wootters, W.K.: Teleporting an unknown quantum state via dual classical and Einstein–Podolsky–Rosen channels. Phys. Rev. Lett. **70**(13), 1895 (1993). https://doi.org/10.1103/PhysRevLett.70.1895
10. Briegel, H.-J., Dür, W., Cirac, J.I., Zoller, P.: Quantum repeaters: the role of imperfect local operations in quantum communication. Phys. Rev. Lett. **81**(26), 5932 (1998). https://doi.org/10.1103/PhysRevLett.81.5932
11. Pan, J.-W., Bouwmeester, D., Weinfurter, H., Zeilinger, A.: Experimental entanglement swapping: entangling photons that never interacted. Phys. Rev. Lett. **80**(18), 3891 (1998). https://doi.org/10.1103/PhysRevLett.80.3891
12. Mafi, Y., Kookani, A., Aghababa, H., Barati, M., Kolahdouz, M.: Quantum broadcasting of the generalized ghz state: quantum noise analysis using quantum state tomography via ibmq simulation. Phys. Scr. **99**(8), 085124 (2024). https://doi.org/10.1088/1402-4896/ad62a9
13. Ahmadkhaniha, A., Mafi, Y., Kazemikhah, P., Aghababa, H., Barati, M., Kolahdouz, M.: Enhancing quantum teleportation: an enable-based protocol exploiting distributed quantum gates. Opt. Quant. Electron. **55**(12), 1079 (2023). https://doi.org/10.1007/s11082-023-05351-1
14. Sadeghi-Zadeh, M.S., Khorrampanah, M., Houshmand, M., Aghababa, H., Mafi, Y.: n-bit quantum secret sharing protocol using quantum secure direct communication. Int. J. Theor. Phys. **60**(10), 3744–3759 (2021). https://doi.org/10.1007/s10773-021-04865-2
15. Taufiqi, M., Purwanto, A., Subagyo, B.A., Sukamto, H., Yuwana, L.: Encrypted quantum controlled teleportation protocol. Int. J. Theor. Phys. **64**(5), 110 (2025). https://doi.org/10.1007/s10773-025-05973-z
16. Yuwana, L., Taufiqi, M., Purwanto, A., Subagyo, B.A., Sukamto, H.: Switch mechanism on a quantum teleportation protocol with dual controllers. Int. J. Theor. Phys. **64**(1), 7 (2025). https://doi.org/10.1007/s10773-024-05877-4
17. Mafi, Y., Kookani, A., Aghababa, H., Barati, M., Kolahdouz, M.: Bidirectional quantum controlled teleportation in multi-hop networks: a generalized protocol for the arbitrary n-qubit state through the noisy channel. Quantum Inf. Process. **23**(10), 350 (2024). https://doi.org/10.1007/s11128-024-04561-0
18. Shi, L.-H., Yu, X.-T., Cai, X.-F., Gong, Y.-X., Zhang, Z.-C.: Quantum information transmission in the quantum wireless multihop network based on werner state. Chin. Phys. B **24**(5), 050308 (2015). https://doi.org/10.1088/1674-1056/24/5/050308

19. Zou, Z.-Z., Yu, X.-T., Gong, Y.-X., Zhang, Z.-C.: Multihop teleportation of two-qubit state via the composite ghz-bell channel. Phys. Lett. A **381**(2), 76–81 (2017). https://doi.org/10.1016/j.physleta.2016.10.048
20. Yang, Y.-L., Yang, Y.-G., Zhou, Y.-H., Shi, W.-M., Li, J.: Efficient quantum multi-hop communication based on Greenberger–Horne–Zeilinger states and bell states. Quantum Inf. Process. **20**(5), 189 (2021). https://doi.org/10.1007/s11128-021-03121-0
21. Zhang, Z., Wang, J., Sun, M.: Multihop teleportation via the composite of asymmetric w state and bell state. Int. J. Theor. Phys. **57**(12), 3605–3620 (2018). https://doi.org/10.1007/s10773-018-3874-4
22. Choudhury, B.S., Samanta, S.: A multi-hop teleportation protocol of arbitrary four-qubit states through intermediate nodes. Int. J. Quantum Inf. **16**(03), 1850026 (2018). https://doi.org/10.1142/S0219749918500260
23. Wu, F., Bai, M.-Q., Tang, L., Mo, Z.-W.: Multi-hop quantum teleportation of an arbitrary two-qubit state based on hierarchical simultaneous entanglement swapping. J. Phys. A Math. Theor. **56**(6), 065301 (2023). https://doi.org/10.1088/1751-8121/acb91d
24. Zhang, Z., Sang, Y.: Bidirectional quantum teleportation in multi-hop communication network. Quantum Inf. Process. **22**(5), 201 (2023). https://doi.org/10.1007/s11128-023-03950-1
25. Yu, X.-T., Xu, J., Zhang, Z.-C.: Distributed wireless quantum communication networks. Chin. Phys. B **22**(9), 090311 (2013). https://doi.org/10.1088/1674-1056/22/9/090311
26. Yu, X.-T., Zhang, Z.-C., Xu, J.: Distributed wireless quantum communication networks with partially entangled pairs. Chin. Phys. B **23**(1), 010303 (2013). https://doi.org/10.1088/1674-1056/23/1/010303
27. Cai, X.-F., Yu, X.-T., Shi, L.-H., Zhang, Z.-C.: Partially entangled states bridge in quantum teleportation. Front. Phys. **9**(5), 646–651 (2014). https://doi.org/10.1007/s11467-014-0432-2
28. Yang, Y.-G., Cao, S.-N., Zhou, Y.-H., Shi, W.-M.: Quantum wireless network communication based on cluster states. Mod. Phys. Lett. A **35**(21), 2050178 (2020). https://doi.org/10.1142/S0217732320501783
29. Nielsen, M.A., Chuang, I.L.: Quantum Computation and Quantum Information. Cambridge University Press, Cambridge (2010)
30. IBM Quantum: ibm_brisbane backend, IBM quantum platform (2025). https://quantum-computing.ibm.com. Accessed 25 June 2025
31. Javadi-Abhari, A., Treinish, M., Krsulich, K., Wood, C.J., Lishman, J., Gacon, J., Martiel, S., Nation, P.D., Bishop, L.S., Cross, A.W., et al.: Quantum computing with Qiskit (2024). Preprint at arXiv:abs/2405.08810. Accessed June 2025
32. Van Den Berg, E., Minev, Z.K., Temme, K.: Model-free readout-error mitigation for quantum expectation values. Phys. Rev. A **105**(3), 032620 (2022). https://doi.org/10.1103/PhysRevA.105.032620
33. Viola, L., Lloyd, S.: Dynamical suppression of decoherence in two-state quantum systems. Phys. Rev. A **58**(4), 2733 (1998). https://doi.org/10.1103/PhysRevA.58.2733
34. Viola, L., Knill, E., Lloyd, S.: Dynamical decoupling of open quantum systems. Phys. Rev. Lett. **82**(12), 2417 (1999). https://doi.org/10.1103/PhysRevLett.82.2417
35. Duan, L.-M., Guo, G.-C.: Suppressing environmental noise in quantum computation through pulse control. Phys. Lett. A **261**(3–4), 139–144 (1999). https://doi.org/10.1016/S0375-9601(99)00592-7
36. Ursin, R., Tiefenbacher, F., Schmitt-Manderbach, T., Weier, H., Scheidl, T., Lindenthal, M., Blauensteiner, B., Jennewein, T., Perdigues, J., Trojek, P., et al.: Entanglement-based quantum communication over 144 km. Nat. Phys. **3**(7), 481–486 (2007). https://doi.org/10.1038/nphys629
37. Yin, J., Ren, J.-G., Lu, H., Cao, Y., Yong, H.-L., Wu, Y.-P., Liu, C., Liao, S.-K., Zhou, F., Jiang, Y., et al.: Quantum teleportation and entanglement distribution over 100-kilometre free-space channels. Nature **488**(7410), 185–188 (2012). https://doi.org/10.1038/nature11332
38. Azuma, K., Economou, S.E., Elkouss, D., Hilaire, P., Jiang, L., Lo, H.-K., Tzitrin, I.: Quantum repeaters: from quantum networks to the quantum internet. Rev. Mod. Phys. **95**(4), 045006 (2023). https://doi.org/10.1103/RevModPhys.95.045006
39. Victora, M., Tserkis, S., Krastanov, S., Cerda, A.S., Willis, S., Narang, P.: Entanglement purification on quantum networks. Phys. Rev. Res. **5**(3), 033171 (2023). https://doi.org/10.1103/PhysRevResearch.5.033171